JACS
JOURNAL OF THE AMERICAN CHEMICAL SOCIETY
Article
pubs.acs.org/JACS

Reversible Substrate Activation and Catalysis at an Intact Metal–Metal Bond Using a Redox-Active Supporting Ligand

Talia J. Steiman and Christopher Uyeda*

Department of Chemistry, Purdue University, West Lafayette, Indiana 47907, United States

Supporting Information

ABSTRACT: An electron rich Ni(I)–Ni(I) bond supported by a doubly reduced naphthyridine–diimine (NDI) ligand reacts rapidly and reversibly with Ph_2SiH_2 and Et_2SiH_2 to form stable adducts. The solid-state structures of these complexes reveal binding modes in which the silanes symmetrically span the Ni–Ni bond and exhibit highly distorted H–Si–H angles and elongated Si–H bonds. This process is facilitated by the release of electron density stored in the π-system of the NDI ligand. Based on this dinuclear mode of activation, [NDI]Ni_2 complexes are shown to catalyze the high-yielding hydrosilylation of alkenes, dienes, alkynes, aldehydes, ketones, enones, and amides. In comparative studies of alkyne hydrosilylations, the [NDI]Ni_2 catalyst is found to be significantly more active than its mononuclear counterparts for aryl-substituted substrates.

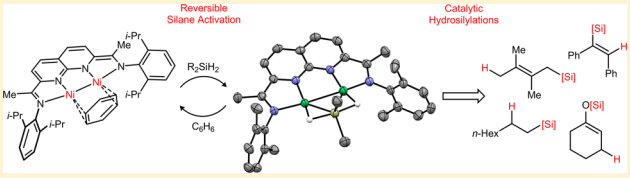

INTRODUCTION

Mononuclear transition metal complexes catalyze a diverse array of organic transformations through sequences of elementary bond breaking and forming steps. Recently, significant interest has been focused on engendering analogous reactivity to complexes of higher nuclearity.[1] These efforts are in part inspired by mechanistic studies of biological and heterogeneous redox catalysts that invoke substrate binding through the direct participation of multiple metal centers.[2] In principle, synthetic catalysts that can capitalize on multimetallic cooperativity effects may exhibit activity or selectivity profiles that diverge from established mononuclear systems, providing access to additional parameters for catalyst design and optimization.

Discrete metal–metal bonds are documented to engage organic substrates and small molecules in stoichiometric redox reactions;[1a,2e,f,3] however, their utility as active sites in catalysis remains relatively unexplored.[4,5] A contributing factor is the limited stability of many metal–metal bonds toward redox processes, causing speciation into mononuclear complexes under turnover conditions.[1a] For example, while Pd(I) dimers have been studied in cross-coupling reactions, in all reported cases, the active species were found to be dissociated monomers.[6] Additionally, in Pd-catalyzed C–H functionalizations, the catalyst is proposed to traverse mononuclear Pd(II) and dinuclear Pd(III)–Pd(III) states, requiring the formation and cleavage of the metal–metal interaction during catalysis.[1g,7] Thus, while group 10 metal–metal bonds can act as precatalysts or transient intermediates, they generally lack the redox flexibility to be maintained during a catalytic cycle.

In order to address this limitation, we recently reported the synthesis of dinuclear Ni complexes using a chelating naphthyridine–diimine (NDI) ligand.[8] The redox-active nature[9] of the NDI π-system allows electron equivalents to be stored in the ligand, leading to Ni–Ni bonds that are stable over an expanded range of oxidation states. Herein, these complexes are shown to promote a rare example of a kinetically facile and reversible substrate activation process across a metal–metal bond. The [NDI]Ni_2 complex **1** bearing a labile C_6H_6 ligand coordinates secondary organosilanes to yield bridging adducts. This dinuclear reactivity provides a complementary pathway to mononuclear Si–H oxidative addition[10] as an entry into catalytic hydrosilylations (Scheme 1). Overall, these results provide the first demonstration that redox-active ligands can enable prototypical organometallic reactions to be catalyzed at an intact metal–metal bond.

Scheme 1. Organosilane Activation Modes Relevant to Catalytic Hydrosilylation Reactions

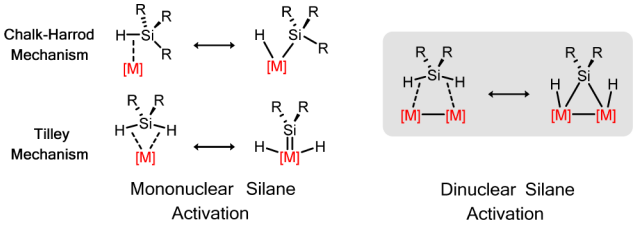

RESULTS AND DISCUSSION

Dinuclear Organosilane Complexes. The [$^{i\text{-Pr}}$NDI]-$Ni_2(C_6H_6)$ complex **1** is readily accessible by combining free $^{i\text{-Pr}}$NDI and $Ni(COD)_2$ (2.0 equiv) in C_6H_6.[8] Complex **1** reacts rapidly with Ph_2SiH_2 (1.0 equiv) in C_6D_6 to form an equilibrium mixture of the silane adduct **2-Ph** (Figure 1a),

Received: March 24, 2015

DOI: 10.1021/jacs.5b03092
J. Am. Chem. Soc. XXXX, XXX, XXX–XXX

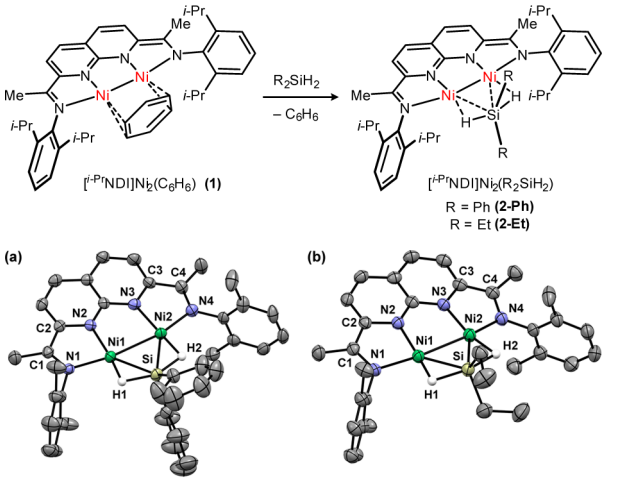

Figure 1. Organosilane binding and solid-state structures of (a) **2-Ph** and (b) **2-Et** (ellipsoids at 50% probability). *i*-Pr groups on the [$^{i\text{-Pr}}$NDI] ligand are truncated for clarity.

free Ph_2SiH_2, and residual **1**. At room temperature, the ^{1}H NMR spectrum exhibits distinct sets of signals for **1** and **2-Ph**, indicating that substitution of Ph_2SiH_2 for C_6D_6 is slow on the NMR chemical shift time scale. In order to confirm the reversibility of Ph_2SiH_2 binding, an equimolar mixture of **1** and Ph_2SiH_2 at an initial concentration of 110 mM was diluted in increments to a final concentration of 7.0 mM (Figure 2). At

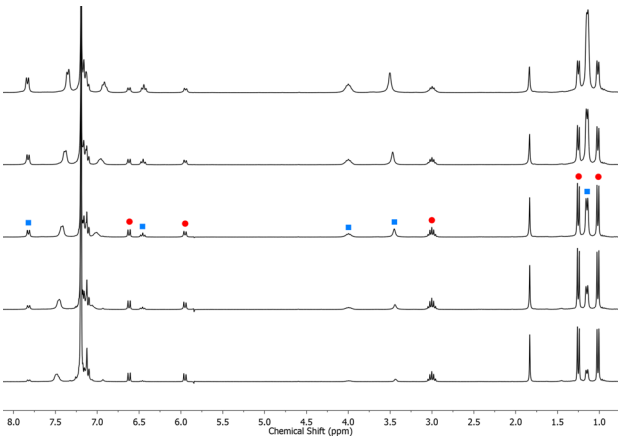

Figure 2. ^{1}H NMR (22 °C, C_6D_6) spectra for the serial dilution of 1:1 [$^{i\text{-Pr}}$NDI]$Ni_2(C_6H_6)$ (**1**) and Ph_2SiH_2: [Ni_2] = 110 mM (bottom) to 7.0 mM (top). Signals assigned to **1** (red circles) and **2-Ph** (blue squares) are labeled.

the highest concentrations, the equilibria favor the silane complex **2-Ph**, whereas **1** predominates under more dilute conditions. Over the range of concentrations examined, a $K_{eq}(Ph_2SiH_2)$ of 420 ± 40 was calculated. Weaker binding is observed using a more electron rich alkyl-substituted silane ($K_{eq}(Et_2SiH_2)$ = 44 ± 2). Tertiary silanes, including Ph_3SiH and Et_3SiH, did not interact to any detectable extent with complex **1**.

At room temperature, **2-Ph** exhibits ^{1}H NMR resonances that are significantly shifted from diamagnetic reference values for free NDI or complex **1**. For example, the signals assigned to the naphthyridine ring appear as broad singlets at −18.0 and +10.6 ppm in THF-d_8 at room temperature. These peaks shift in a temperature-dependent fashion, suggesting that **2-Ph** has a diamagnetic ground state with a thermally populated paramagnetic excited state. For **2-Ph**, the difference in energy between the ground state and excited state is too small to accurately determine a value by modeling the NMR data over the accessible temperature range; however, for **2-Et**, a singlet−triplet gap of 2.8 kcal/mol was calculated by fitting the naphthyridine chemical shifts from spectra acquired in the range of +22 to −64 °C (Figure 3a). The accessibility of higher

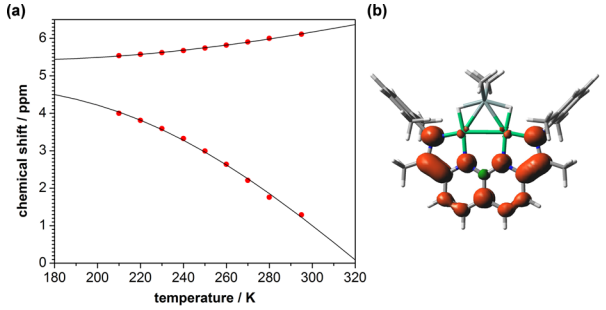

Figure 3. (a) Variable temperature ^{1}H NMR chemical shifts (red circles) for the two naphthyridine doublet signals of **2-Et**. Data were modeled by taking into account a Boltzmann population of a triplet excited state (see Supporting Information for the fitting function).[2g,12] From the best fits, a singlet−triplet gap of 2.8 kcal/mol and chemical shifts for the diamagnetic state of 5.4 and 4.8 ppm were calculated. (b) Calculated spin density plot for the triplet state of a model dimethylsilane complex (B3LYP/6-311+G(d,p)).

spin states for the silane complexes as compared to **1**, which is diamagnetic at all examined temperatures (up to 80 °C), likely reflects the weaker field strength of the silane ligand relative to C_6H_6. Notably, this variable temperature behavior contrasts with the temperature-independent paramagnetism observed by Chirik for related (pyridine−diimine)Fe complexes.[9b,11]

Diffusion of pentane vapor into saturated solutions of the [$^{i\text{-Pr}}$NDI]$Ni_2(C_6H_6)$ complex **1** dissolved in excess Ph_2SiH_2 yielded crystalline samples of the silane complex **2-Ph** that were suitable for X-ray diffraction analysis. The solid-state structure (Figure 1a and Table 1) reveals that Ph_2SiH_2 symmetrically

Table 1. Selected Bond Metrics (Å) from Solid-State Structures

	2-Ph[a]	2-Et	3
Ni1−Ni2	2.6284(9), 2.5625(9)	2.5545(6)	2.4500(7)
Ni1−Si	2.258(1), 2.263(1)	2.268(1)	2.335(1)
Ni2−Si	2.228(2), 2.222(2)	2.2559(9)	2.170(1)
Ni1−H1	1.51(4), 1.59(5)	1.51(4)	1.56(3)
Ni2−H2	1.53(4), 1.49(6)	1.54(4)	
Si−H1	1.55(3), 1.56(5)	1.61(4)	1.66(3)
Si−H2	1.65(5), 1.57(7),	1.67(4)	

[a]Two molecules in the asymmetric unit. Metrics for both are shown.

bridges the two Ni atoms[13] with Ni−Si distances (2.243(2) Å for two molecules in the asymmetric unit) that are within the range of structurally characterized mononuclear Ni(silyl) complexes.[14] The μ-H atoms were located in the difference map and refined to an average Ni−H distance of 1.53(5) Å and Si−H distance of 1.58(5) Å. A remarkable structural feature of **2-Ph** is the highly distorted H−Si−H angle of 156(3)°. An analogous silane adduct was obtained using Et_2SiH_2 (Figure 1b). The weaker binding of Et_2SiH_2 to the [$^{i\text{-Pr}}$NDI]Ni_2

DOI: 10.1021/jacs.5b03092
J. Am. Chem. Soc. XXXX, XXX, XXX−XXX

platform in solution is manifested in the solid state by longer Ni–Si distances and a correspondingly shorter Ni–Ni distance as compared to **2-Ph**.

In both **2-Ph** and **2-Et**, the μ-H atoms are nearly equidistant between Ni and Si, suggesting that these adducts are intermediate structures between the limiting cases of a σ-complex and a μ-silylene dihydride derived from a double oxidative addition process (Scheme 1). The Ni–H–Si bonding arrangement found in these complexes is reminiscent of similar three-center-two-electron bonds described by Hillhouse for a mononuclear (diphosphine)Ni(μ-H)($SiMes_2$)$^+$ complex.[14d]

Electronic Structure and Computational Models. In order to gain further insight into the nature of the interaction between the Ni–Ni bond and secondary organosilanes, DFT calculations were conducted on a model S = 0 Me_2SiH_2 complex (B3LYP/6-311+G(d,p)). The triplet state was also calculated and found to be 8.3 kcal/mol higher in energy. The computationally optimized structure closely reproduces the symmetrical silane binding mode and experimental bond metrics for **2-Et** (see Supporting Information for a comparison of the bond metrics).

Orbitals with significant Ni–Si and Ni–H bonding character were located at HOMO−15 and HOMO−17 respectively (Figure 4a). These orbitals arise from mixing between the d_{xy}–

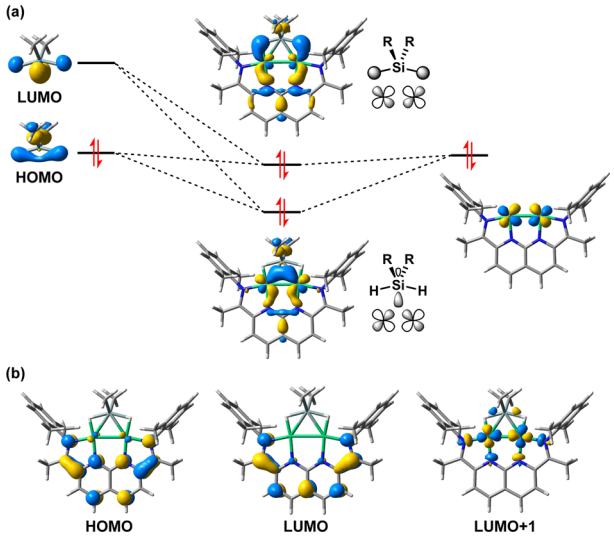

Figure 4. Selected Kohn–Sham orbitals (B3LYP/6-311+G(d,p)) for a model dimethylsilane complex (S = 0) highlighting (a) interactions between the Ni_2 and Me_2SiH_2 fragments and (b) frontier orbitals.

d_{xy} π orbital of the Ni–Ni bond and the HOMO and the LUMO for the silane in its distorted geometry (A_1 symmetry in C_{2v}). The calculated net Ni–H and Si–H bond orders according to the natural bond orbital (NBO) Wiberg bond index are 0.41 and 0.47, respectively, corresponding to an approximately symmetrical bonding of the μ-H to Ni and Si. This analysis implicates back-donation from the filled Ni–Ni π-bonding orbital into the unfilled H–Si–H antibonding orbital as a significant contributor to the silane binding energy. The stronger binding affinity of Ph_2SiH_2 and the longer Ni–Ni distance in **2-Ph** as compared to **2-Et** are rationalized by this model.

The calculated HOMO is a primarily ligand-centered π orbital, and the Ni–Ni σ* orbital (LUMO + 1) is unoccupied (Figure 4b). The electronic configuration by NBO analysis indicates a d^9–d^9 electron count for the Ni–Ni bond. Overall, the calculations are most consistent with a $[NDI]^{2-}$ and Ni(I)–Ni(I) oxidation state assignment for the C_6H_6 and silane complexes. For the triplet state, the two unpaired electrons occupy the two primarily ligand-centered π orbitals (HOMO and LUMO in Figure 4b), and by Mulliken population analysis, the spin density (Figure 3b) is nearly entirely localized on the NDI ligand atoms.

In support of the calculated electronic structure model, the experimental bond metrics associated with the NDI ligand of **2-Et** exhibit typical features of ligand-centered reduction: elongated imine C–N and napthyridine C_{ipso}–N distances and contracted C_{ipso}–C_{imine} distances. Notably, the degree of NDI reduction is highly responsive to the identity of the substrate bound to the Ni–Ni bond (Figure 5). For example,

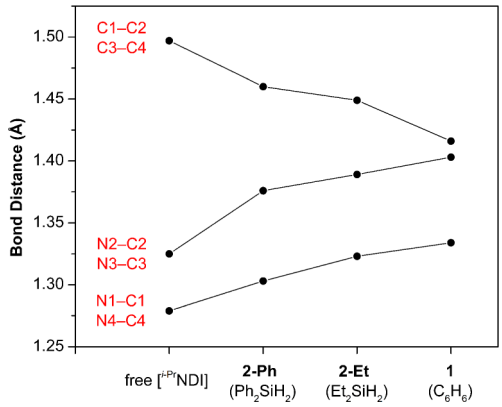

Figure 5. Summary of [$^{i\text{-Pr}}$NDI] bond metrics sensitive to ligand-centered reduction. In all structures, the bond distances observed for the two halves of the ligand are approximately equivalent. Average values are plotted. The numbering scheme is shown in Figure 1.

the NDI ligand appears to be in a more oxidized state in **2-Ph** than in **2-Et**. For both silane complexes, the NDI ligand is more oxidized than that for the C_6H_6 adduct **1**. Taken together, these structural trends demonstrate that donation of electron density stored in the NDI π-system plays a significant role in promoting the binding and activation of organosilanes at the Ni_2 fragment. Overall, the degree of ligand-centered reduction is inversely correlated with the measured binding preference of Ph_2SiH_2 > Et_2SiH_2 > C_6H_6.

Hydride Transfer Reactivity. Under the crystallization conditions described above for **2-Ph**, an additional species **3** was identified by XRD (Figure 6). The isomeric complex features a silyl ligand bound to one Ni center with a secondary agostic interaction of the Si–H bond to the adjacent Ni. By ^{1}H NMR, a sharp singlet, sensitive to labeling with Ph_2SiD_2, is

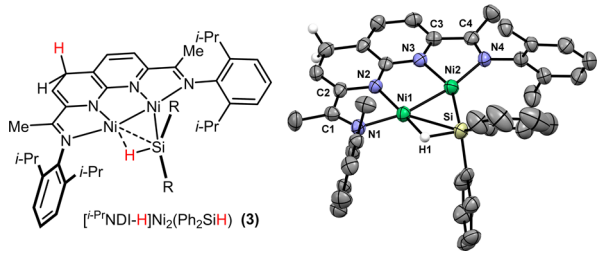

Figure 6. Solid-state structure of **3** (ellipsoids at 50% probability). *i*-Pr groups on the [$^{i\text{-Pr}}$NDI] ligand are truncated for clarity.

DOI: 10.1021/jacs.5b03092
J. Am. Chem. Soc. XXXX, XXX, XXX–XXX

observed at −16.1 ppm (THF-d_8). Dearomatization of one of the rings in the naphthyridine system is evident in the dihydropyridine-like distortions in the C−C and C−N distances. Additionally, the two hydrogens bound to the sp^3-hybridized carbon were located in the difference map. It is noteworthy that this isomeric product was not formed in reactions between **1** and Et_2SiH_2.

Complex **3** is generated when **1** is stored in neat Ph_2SiH_2; however, in C_6D_6 solution, this reaction does not occur even after heating at 60 °C over 24 h. This concentration dependence is highly suggestive that **3** does not arise from an intramolecular rearrangement, but rather, a higher kinetic order intermolecular process. When stored as a C_6D_6 solution, **3** reverts back to **1** over the course of days at room temperature. The formation of **3** provides evidence that this system facilitates hydride transfer from a silane to an organic fragment.

Catalytic Hydrosilylation of 1-Octene. Hydrosilylations catalyzed by group 10 transition metal complexes are generally proposed to proceed by variants of the Chalk-Harrod mechanism (Scheme 1), where oxidative addition of a Si−H bond leads to a Si−M−H intermediate. While such oxidative additions at Pt are well-precedented[15]—indeed, Pt complexes are often used as industrial hydrosilylation catalysts—examples at Ni are relatively uncommon. Reported cases either utilize strongly donating ligands, such as alkylphosphines[14c,16] and NHCs,[14b] or ligands that incorporate pendant Lewis acidic functionality to assist in the Si−H bond cleavage.[17] The facile silane activation observed by the [NDI]Ni_2 platform demonstrates that Ni complexes of less electron rich N-donor ligands can nonetheless engage organosilane substrates by taking advantage of binding across multiple metal centers.

Based on these observations, we next examined the propensity of complex **1** to catalyze a model hydrosilylation reaction (Scheme 2). While other examples of dinuclear Ni complexes bearing bridging silane or silyl ligands have been reported, their relevance to catalytic hydrosilylation has not been explored.[13,18] At 5 mol % loading of **1**, the hydrosilylation of 1-octene with Ph_2SiH_2 proceeds to >95% conversion in 22 h at room temperature, producing the hydrosilylated product in 77% yield. Et_2SiH_2 reacts more slowly, yielding only 35% of the product after the same reaction time with significant unreacted 1-octene. The relative rate of hydrosilylation with Ph_2SiH_2 and Et_2SiH_2 presumably reflects the weaker binding constant for Et_2SiH_2. Tertiary silanes, which do not bind to complex **1**, were unreactive in hydrosilylation reactions even after heating at 60 °C for 24 h.

Scheme 2. Catalytic Hydrosilylation of 1-Octene with Ph_2SiH_2

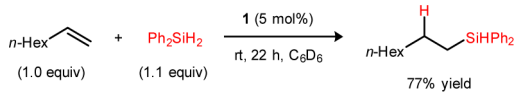

During catalytic hydrosilylations between 1-octene and Ph_2SiH_2 in C_6D_6, the silane complex **2-Ph** can be directly observed by ^{1}H NMR as the primary catalyst resting state. As Ph_2SiH_2 is depleted at higher conversions, the equilibrium shifts toward **1**. During the reaction course, there is no change in the total catalyst concentration (the sum of **1** and **2-Ph**), indicating minimal catalyst decomposition. The presence of elemental Hg also does not cause inhibition of the reaction. The isomeric complex **3** is not formed within the limit of detection. Coupled with the lack of a catalyst induction period, this observation suggests that **3** is likely not relevant to the mechanism of catalysis.

Substrate Scope for Catalytic Hydrosilylations. Complex **1** exhibits a broad substrate scope for the catalytic hydrosilylation of carbon−carbon and carbon−oxygen multiple bonds (Table 2). For aliphatic alkenes such as 1-octene, the anti-Markovnikov product is formed exclusively. By contrast, styrene yields an approximately 1:1 mixture of regioisomers. Dienes undergo highly selective 1,4-hydrosilylation to form the corresponding allyl silane products. The reaction of isoprene is particularly efficient, proceeding to complete conversion in 1 h at room temperature with 1 mol % loading of catalyst **1**. Internal alkynes containing alkyl or aryl substituents are hydrosilylated in a syn fashion to yield (*E*)-alkene products.

Table 2. Substrate Scope for Catalytic Hydrosilylations with 1[a]

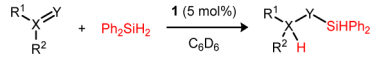

substrate	product	time / temp	yield
	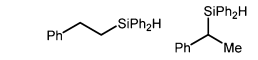 1 + 1.1	8 h / rt	94%
	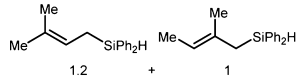 1.2 + 1	1 h / rt	97%[b]
	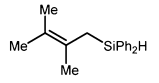	12 h / rt	98%
	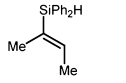	1.5 h / rt	93%
	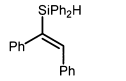	3.5 h / rt	93%
		24 h / rt	88%
	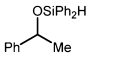	24 h / 60 °C	97%
	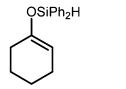	14 h / rt	99%
	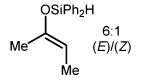 6:1 (*E*)/(*Z*)	15 min / rt	99%
	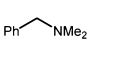	48 h / 60 °C	76%[c]

[a]Reactions were conducted in C_6D_6 with 1.0 equiv of the substrate, 1.1 equiv of Ph_2SiH_2, and 5 mol % of **1**. Yields were averaged over two runs and determined by ^{1}H NMR integration against an internal standard. [b]Reaction was conducted with 1 mol % of **1**. [c]Reaction was conducted with 4.0 equiv of Ph_2SiH_2.

More polar substrates, including aldehydes and ketones, are also hydrosilylated by catalyst **1**. Cyclic and acyclic enones undergo 1,4-hydrosilylation. In the case of methyl vinyl ketone, the *E* stereoisomer is favored. Finally, *N*,*N*-dimethylbenzamide is reductively deoxygenated to *N*,*N*-dimethylbenzylamine in 77% yield using an excess of Ph_2SiH_2.

DOI: 10.1021/jacs.5b03092
J. Am. Chem. Soc. XXXX, XXX, XXX−XXX

The scope of substrates that are efficiently hydrosilylated by the dinuclear complex **1** is noteworthy in comparison to reported mononuclear Ni catalysts.[17,19] In particular, common side products arising from dehydrogenative silylation or silylative C−C coupling were not formed using catalyst **1**.[19a,i−l] In cases where the yields are less than quantitative, products arising from Ph_2SiH_2 redistribution to $PhSiH_3$ and Ph_3SiH were observed. For example, with 1-octene, Ph_3SiH, and $(C_8H_{17})_2PhSiH$ were identified by GC/MS. In a majority of cases, however, hydrosilylation is sufficiently rapid to outcompete the redistribution process. Tetrasubstituted silane products are not formed for any substrate class, consistent with the lack of reactivity with tertiary silanes.

Catalyst Nuclearity Effects in Alkyne Hydrosilylations. Motivated by the fast rate and high efficiency of alkyne hydrosilylations using **1**, we undertook a comparative study with analogous mononuclear Ni catalysts containing chelating N-donor ligands. The relatively electron rich 2,2′-bipyridine complex **4** and the more hindered and electron deficient α-diimine complex **5** were selected as comparison compounds. For 2-butyne (Table 3, entries 1−3), [bpy]Ni(COD) (**4**)

Table 3. Comparison of Mononuclear and Dinuclear Ni Catalysts for the Hydrosilylation of Alkynes[a]

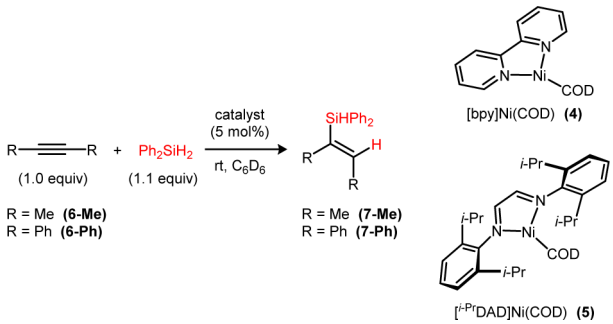

entry	substrate	catalyst	yield of 7
1	**6-Me**	**1**	**93%**
2	6-Me	**4**	77%
3	6-Me	**5**	<1%
4	**6-Ph**	**1**	**93%**
5	6-Ph	**4**	<1%
6	6-Ph	**5**	<1%

[a]Reactions were conducted in C_6D_6 with 1.0 equiv of the alkyne substrate, 1.1 equiv of Ph_2SiH_2, and 5 mol % of the catalyst. For **6-Me**, the reaction was run for 1.5 h, and for **6-Ph**, the reaction was run for 3.5 h. Yields were averaged over two runs and determined by ^1H NMR integration against an internal standard.

exhibits a similar reaction rate to **1** with a slightly diminished yield due to the competing formation of tetrasubstituted silanes and hydrogenated alkyl silane side products.

For diphenylacetylene, the dinuclear catalyst **1** is significantly more active than either mononuclear catalyst. After 3.5 h, 93% yield of the hydrosilylated product is obtained with **1**. There is no detectable conversion using **4** under otherwise identical conditions (approximately 40% yield after 11 d at room temperature). While the origin of this effect requires more detailed mechanistic studies, preliminary observations suggest that **4** forms a stable alkyne complex[20] that persists under catalytic conditions. A plausible rationale for this low activity is the unfavorable alkyne dissociation that would be required for silane activation.

CONCLUSIONS

In summary, metal−metal bonds supported by a redox-active ligand are shown to be viable platforms for stoichiometric bond activations and for catalytic processes. The doubly reduced $[NDI]^{2-}$ ligand in complex **1** affords a sufficiently electron-rich Ni(I)−Ni(I) bond that secondary organosilanes coordinate reversibly to form symmetrically bridging species. These adducts fall on the continuum between a σ-complex and a product of double Si−H oxidative addition. The lack of reactivity with tertiary organosilanes suggests that interactions with both Ni atoms are required for this binding to be favorable. Structural studies in combination with relative binding constant measurements are consistent with a significant release of electron density from the NDI π-system upon silane coordination.

This dinuclear mode of silane activation provides a complementary mechanism to mononuclear Si−H oxidative additions as a means of promoting catalytic hydrosilylation. Thus, complex **1** catalyzes the high-yielding addition of Ph_2SiH_2 to a broad range of organic substrates. Preliminary data comparing the dinuclear complex to analogous mononuclear complexes in alkyne hydrosilylations reveal distinct rate advantages for aryl-substituted substrates. Overall, these results provide a promising indication that nuclearity is a parameter that can be exploited for catalyst optimization. Ongoing studies are aimed at elucidating the origin of these effects and extending these principles to other catalytic processes.

EXPERIMENTAL SECTION

General Considerations. All manipulations were carried out using standard Schlenk or glovebox techniques under an atmosphere of N_2 unless otherwise noted. Solvents were dried and degassed by passage through a column of activated alumina and sparging with Ar gas. Deuterated solvents were purchased from Cambridge Isotope Laboratories, Inc., degassed, and stored over activated 3 Å molecular sieves prior to use. All other reagents and starting materials were purchased from commercial vendors and used without further purification unless otherwise noted. Liquid reagents were degassed and stored over activated 3 Å molecular sieves prior to use. Elemental analyses were performed by Midwest Microlab (Indianapolis, IN). The $[^{i\text{-}Pr}NDI]Ni_2(C_6H_6)$ complex **1** was prepared according to previously reported procedures.[8]

Physical Methods. ^1H and ^2H NMR spectra were collected on Varian INOVA 300 MHz and Varian INOVA 600 MHz NMR spectrometers. ^{13}C NMR spectra were collected at room temperature on Bruker ARX400 and Bruker AV-III-500-HD spectrometers. Variable temperature ^1H NMR spectra were collected on both Varian INOVA 300 MHz and Bruker DRX500 spectrometers. ^1H and ^{13}C NMR spectra are reported in parts per million relative to tetramethylsilane, using the residual solvent resonances as an internal standard. GC/MS data was collected on a Shimadzu GC-2010/MS-QP2010 spectrometer containing a mini-bore capillary GC column and single quad EI detector. ATR-IR data were collected on a Thermo Nicolet Nexus spectrometer containing a MCT* detector and KBr beam splitter with a range of 350−7400 cm^{-1}. UV−vis measurements were acquired on a Cary 100 UV/vis spectrophotometer using a 1 cm two-window quartz cuvette.

X-ray Crystallography. Single-crystal X-ray diffraction studies were carried out at the Purdue X-ray crystallography facility on either a Nonius KappaCCD or Rigaku Rapid II diffractometer. Data were collected at 150 or 200 K using Mo Kα (λ = 0.71073 Å) or Cu Kα (λ = 1.54178 Å) radiation. Structures were solved using direct methods using SHELXT and refined against F2 on all data by full-matrix least-squares.

Computational Methods. DFT calculations were performed with the Gaussian 09 software package. The geometry of a model

DOI: 10.1021/jacs.5b03092
J. Am. Chem. Soc. XXXX, XXX, XXX−XXX

[^{Me}NDI]Ni$_2$(Me$_2$SiH$_2$) and isomeric [^{Me}NDI-H]Ni$_2$(Me$_2$SiH) complex was fully optimized at the B3LYP/6-311+G(d,p) level of DFT[21] using the XRD coordinates of **2-Et** and **3** as a input geometries. The stationary points were verified by frequency analysis. A comparison of the calculated and experimental bond distances from the XRD structure for **2-Et** is included in the Supporting Information.

[$^{i\text{-Pr}}$NDI]Ni$_2$(Ph$_2$SiH$_2$) (2-Ph) and [$^{i\text{-Pr}}$NDI-H]Ni$_2$(Ph$_2$SiH) (3). A 20 mL vial was charged with [$^{i\text{Pr}}$NDI]Ni$_2$(C$_6$H$_6$) (**1**) (25 mg, 0.034 mmol, 1.0 equiv) and Ph$_2$SiH$_2$ (6.4 μL, 0.034 mmol, 1.0 equiv). Diethyl ether (2.0 mL) was added, and the reaction was stirred until a golden brown homogeneous solution was obtained. The solvent was removed under reduced pressure. The residue was redissolved in diethyl ether (2.0 mL), and the resulting solution was concentrated to dryness under vacuum to produce 29 mg of an inseparable mixture of [$^{i\text{-Pr}}$NDI]Ni$_2$(Ph$_2$SiH$_2$) (**2-Ph**) (94% yield) and [$^{i\text{-Pr}}$NDI-H]-Ni$_2$(Ph$_2$SiH) (**3**) (5% yield). Elemental analysis data for the mixture of isomers is shown below. A crystalline sample suitable for XRD analysis was obtained by slow diffusion of pentane vapor into the mixture of products dissolved in THF (approximately 100 μL containing one drop of Ph$_2$SiH$_2$). The crystalline material obtained by this procedure was analyzed by ^{1}H NMR and determined to be a 1:1.2 ratio of **2-Ph** and **3**. NMR and UV−vis data for **2-Ph** were obtained by combining **1** and Ph$_2$SiH$_2$ in a 1:1 ratio in THF. NMR data for **3** were obtained from the crystalline mixture of **2-Ph** and **3**. Data for **2-Ph**: ^{1}H NMR (300 MHz, 22 °C, THF-d_8) δ 10.64 (s, 2 H), 8.31 (d, J = 7.4 Hz, 4 H), 7.13−7.00 (m, 6 H), 6.98−6.86 (m, 4 H), 6.01 (t, J = 7.5 Hz, 2 H), 5.45 (s, 6 H), 4.10 (s, 4 H), 1.16 (d, J = 6.1 Hz, 12 H), 0.98 (d, J = 5.6 Hz, 12 H), −17.96 (s, 2 H). UV−vis (THF): λ (nm) {ε, cm^{-1} M^{-1}} 453 {860}, 363 {18 000}, 271 {27 000}. Data for **3**: ^{1}H NMR (300 MHz, 22 °C, C$_6$D$_6$) δ 7.55 (d, J = 7.0 Hz, 4 H), 7.15−7.07 (m, 6 H), 7.05−6.92 (m, 6 H), 6.38 (d, J = 7.2 Hz, 1 H), 6.09 (d, J = 7.1 Hz, 1 H), 4.87 (t, J = 4.2 Hz, 1 H), 3.58 (sept, J = 6.7 Hz, 2 H), 3.39−3.24 (m, 4 H), 1.38 (s, 3 H), 1.16 (d, J = 6.7 Hz, 6 H), 1.11 (d, J = 6.7 Hz, 6 H), 1.09 (s, 3 H), 1.02 (d, J = 6.9 Hz, 6 H), 0.98 (d, J = 6.8 Hz, 6 H), −15.59 (s, 1 H). Anal. Calcd for **2-Ph** and **3** (C$_{48}$H$_{56}$N$_4$Ni$_2$Si): C, 69.09; H, 6.76; N, 6.71. Found: C, 69.12; H, 6.64; N, 6.64.

[$^{i\text{-Pr}}$NDI]Ni$_2$(Et$_2$SiH$_2$) (2-Et). A 20 mL vial was charged with [$^{i\text{-Pr}}$NDI]Ni$_2$(C$_6$H$_6$) (**1**) (20 mg, 0.028 mmol, 1.0 equiv) and Et$_2$SiH$_2$ (50 μL, 0.39 mmol, 14 equiv). Diethyl ether (2.0 mL) was added, and the reaction was stirred at room temperature for 30 min to produce a golden brown homogeneous solution. The solvent was removed under reduced pressure. To ensure complete ligand exchange, the residue was redissolved in diethyl ether (2.0 mL) and a second portion of Et$_2$SiH$_2$ (50 μL, 0.39 mmol, 14 equiv) was added. After stirring at room temperature for 30 min, the solution was concentrated to dryness under vacuum to produce [$^{i\text{-Pr}}$NDI]Ni$_2$(Et$_2$SiH$_2$) (**2-Et**) (20 mg, 99% yield). Single crystals suitable for XRD were obtained by diffusion of pentane vapor into a concentrated solution of **2-Et** in THF. ^{1}H NMR (300 MHz, 22 °C, THF-d_8) δ 7.22−7.16 (m, 4 H), 6.82 (t, J = 7.7 Hz, 2 H), 6.14 (d, J = 7.6 Hz, 2 H), 3.62−3.49 (m, 4 H), 1.77 (s, 6 H), 1.32 (d, J = 6.8 Hz, 12 H), 1.16 (d, J = 6.8 Hz, 12 H), 1.13−0.99 (m, 6 H), 0.66 (t, J = 7.4 Hz, 6 H). Anal. Calcd for **2-Et** (C$_{40}$H$_{56}$N$_4$Ni$_2$Si): C, 65.07; H, 7.64; N, 7.59. Found: C, 64.91; H, 7.79; N, 7.31.

Equilibrium Constant Measurements. A 1:1 ratio of [$^{i\text{Pr}}$NDI]-Ni$_2$(C$_6$H$_6$) (**1**) and R$_2$SiH$_2$ were combined in C$_6$D$_6$ (0.5 mL) at initial concentrations of 110 mM for R = Ph and 165 mM for R = Et. The ^{1}H NMR spectra were recorded, and 2-fold dilutions were performed by removing 0.25 mL of the solution and adding 0.25 mL of C$_6$D$_6$. Solutions were diluted to final concentrations of 7.0 mM for R = Ph and 10 mM for R = Et. Equilibrium constants were determined from the ratios of **1** and **2**. Values at each concentration were averaged: K_{eq}(Ph$_2$SiH$_2$) = 420 ± 40 and K_{eq}(Et$_2$SiH$_2$) = 44 ± 2.

Catalytic Hydrosilylation of 1-Octene with Ph$_2$SiH$_2$. 1-Octene (15 mg, 0.13 mmol, 1.0 equiv), Ph$_2$SiH$_2$ (27 mg, 0.14 mmol, 1.1 equiv), [$^{i\text{-Pr}}$NDI]Ni$_2$(C$_6$H$_6$) (**1**) (4.8 mg, 0.0067 mmol, 5.0 mol %), and mesitylene (16 mg, 0.13 mmol, 1.0 equiv) in C$_6$D$_6$ (0.5 mL) were allowed to react for 22 h at room temperature. The yield of octyldiphenylsilane was determined to be 77% by ^{1}H NMR integration against mesitylene. ^{1}H NMR (300 MHz, 22 °C, C$_6$D$_6$) δ 7.61−7.54 (m, 4 H), 7.20−7.15 (m, 6 H), 5.14 (t, J = 3.6 Hz, 1 H), 1.59−1.49 (m, 2 H), 1.43−1.22 (m, 10 H), 1.21−1.09 (m, 2 H), 0.95 (t, J = 6.7 Hz, 3 H).

Comparison of Catalyst Activity in Alkyne Hydrosilylations. The alkyne (0.13 mmol, 1.0 equiv), Ph$_2$SiH$_2$ (0.14 mmol, 1.1 equiv), [$^{i\text{-Pr}}$NDI]Ni$_2$(C$_6$H$_6$) (**1**) (0.0065 mmol, 5.0 mol %), and mesitylene (0.13 mmol, 1.0 equiv) in C$_6$D$_6$ (0.5 mL) were allowed to react at room temperature. After 1.5 h for 2-butyne or 3.5 h for diphenylacetylene, yields of the hydrosilylated products were determined by ^{1}H NMR integration against mesitylene.

■ ASSOCIATED CONTENT

Supporting Information

Experimental procedures, spectra, crystallographic details, and calculated structures. The Supporting Information is available free of charge on the ACS Publications website at DOI: 10.1021/jacs.5b03092.

■ AUTHOR INFORMATION

Corresponding Author

*cuyeda@purdue.edu

Notes

The authors declare no competing financial interest.

■ ACKNOWLEDGMENTS

This work was generously supported by Purdue University. We thank Dr. Phillip Fanwick and Ian Powers for assistance with X-ray crystallography.

■ REFERENCES

(1) For examples of reactivity studies with group 10 metal−metal bonds: (a) Velian, A.; Lin, S.; Miller, A. J. M.; Day, M. W.; Agapie, T. *J. Am. Chem. Soc.* **2010**, *132*, 6296−6297. (b) Lin, S.; Herbert, D. E.; Velian, A.; Day, M. W.; Agapie, T. *J. Am. Chem. Soc.* **2013**, *135*, 15830−15840. (c) Lin, S.; Agapie, T. *Synlett* **2011**, *2011*, 1−5. (d) Keen, A. L.; Johnson, S. A. *J. Am. Chem. Soc.* **2006**, *128*, 1806−1807. (e) Beck, R.; Johnson, S. A. *Chem. Commun.* **2011**, *47*, 9233−9235. (f) Powers, D. C.; Ritter, T. *Acc. Chem. Res.* **2011**, *45*, 840−850. (g) Powers, D. C.; Ritter, T. *Nat. Chem.* **2009**, *1*, 302−309. (h) DeLaet, D. L.; Del Rosario, R.; Fanwick, P. E.; Kubiak, C. P. *J. Am. Chem. Soc.* **1987**, *109*, 754−758. (i) Laskowski, C. A.; Hillhouse, G. L. *Chem. Sci.* **2011**, *2*, 321−325.

(2) For select recent discussions of multinuclear functional models of metalloenzymes: (a) Chang, C. J.; Loh, Z.-H.; Shi, C.; Anson, F. C.; Nocera, D. G. *J. Am. Chem. Soc.* **2004**, *126*, 10013−10020. (b) Collman, J. P.; Boulatov, R.; Sunderland, C. J.; Fu, L. *Chem. Rev.* **2004**, *104*, 561−588. (c) Kanady, J. S.; Tsui, E. Y.; Day, M. W.; Agapie, T. *Science* **2011**, *333*, 733−736. (d) Park, Y. J.; Ziller, J. W.; Borovik, A. S. *J. Am. Chem. Soc.* **2011**, *133*, 9258−9261. (e) Krogman, J. P.; Foxman, B. M.; Thomas, C. M. *J. Am. Chem. Soc.* **2011**, *133*, 14582−14585. (f) Powers, T. M.; Betley, T. A. *J. Am. Chem. Soc.* **2013**, *135*, 12289−12296. (g) Rittle, J.; McCrory, C. C. L.; Peters, J. C. *J. Am. Chem. Soc.* **2014**, *136*, 13853−13862.

(3) (a) Thomas, C. M.; Napoline, J. W.; Rowe, G. T.; Foxman, B. M. *Chem. Commun.* **2010**, *46*, 5790−5792. (b) Powers, T. M.; Fout, A. R.; Zheng, S.-L.; Betley, T. A. *J. Am. Chem. Soc.* **2011**, *133*, 3336−3338. (c) Hruszkewycz, D. P.; Wu, J.; Hazari, N.; Incarvito, C. D. *J. Am. Chem. Soc.* **2011**, *133*, 3280−3283.

(4) (a) Gibson, S. E.; Stevenazzi, A. *Angew. Chem., Int. Ed.* **2003**, *42*, 1800−1810. (b) Magnus, P.; Principe, L. M. *Tetrahedron Lett.* **1985**, *26*, 4851−4854. (c) Cooper, B. G.; Napoline, J. W.; Thomas, C. M. *Catal. Rev.* **2012**, *54*, 1−40.

(5) For examples of carbene transfer using Rh$_2$ catalysts: (a) Doyle, M. P.; Duffy, R.; Ratnikov, M.; Zhou, L. *Chem. Rev.* **2010**, *110*, 704−724. (b) Davies, H. M. L.; Morton, D. *Chem. Soc. Rev.* **2011**, *40*, 1857−1869. (c) Kornecki, K. P.; Berry, J. F.; Powers, D. C.; Ritter, T. In

DOI: 10.1021/jacs.5b03092
J. Am. Chem. Soc. XXXX, XXX, XXX−XXX

Progress in Inorganic Chemistry; Karlin, K. D., Ed.; John Wiley & Sons, Inc.: New York, 2014; Vol. *58*, pp 225−302. (d) Kornecki, K. P.; Berry, J. F. *Eur. J. Inorg. Chem.* **2012**, *2012*, 562−568. (e) Sarkar, M.; Daw, P.; Ghatak, T.; Bera, J. K. *Chem.—Eur. J.* **2014**, *20*, 16537−16549.

(6) (a) Barder, T. E. *J. Am. Chem. Soc.* **2005**, *128*, 898−904. (b) Hruszkewycz, D. P.; Balcells, D.; Guard, L. M.; Hazari, N.; Tilset, M. *J. Am. Chem. Soc.* **2014**, *136*, 7300−7316. (c) Christmann, U.; Pantazis, D. A.; Benet-Buchholz, J.; McGrady, J. E.; Maseras, F.; Vilar, R. *J. Am. Chem. Soc.* **2006**, *128*, 6376−6390.

(7) Powers, D. C.; Geibel, M. A. L.; Klein, J. E. M. N.; Ritter, T. *J. Am. Chem. Soc.* **2009**, *131*, 17050−17051.

(8) Zhou, Y.-Y.; Hartline, D. R.; Steiman, T. J.; Fanwick, P. E.; Uyeda, C. *Inorg. Chem.* **2014**, *53*, 11770−11777.

(9) (a) Bouwkamp, M. W.; Bowman, A. C.; Lobkovsky, E.; Chirik, P. J. *J. Am. Chem. Soc.* **2006**, *128*, 13340−13341. (b) Bart, S. C.; Chłopek, K.; Bill, E.; Bouwkamp, M. W.; Lobkovsky, E.; Neese, F.; Wieghardt, K.; Chirik, P. J. *J. Am. Chem. Soc.* **2006**, *128*, 13901−13912. (c) Lu, C. C.; Bill, E.; Weyhermüller, T.; Bothe, E.; Wieghardt, K. *J. Am. Chem. Soc.* **2008**, *130*, 3181−3197.

(10) (a) Chalk, A. J.; Harrod, J. F. *J. Am. Chem. Soc.* **1965**, *87*, 16−21. (b) Glaser, P. B.; Tilley, T. D. *J. Am. Chem. Soc.* **2003**, *125*, 13640−13641.

(11) (a) Bart, S. C.; Bowman, A. C.; Lobkovsky, E.; Chirik, P. J. *J. Am. Chem. Soc.* **2007**, *129*, 7212−7213. (b) Bart, S. C.; Lobkovsky, E.; Bill, E.; Wieghardt, K.; Chirik, P. J. *Inorg. Chem.* **2007**, *46*, 7055−7063. (c) Trovitch, R. J.; Lobkovsky, E.; Bill, E.; Chirik, P. J. *Organometallics* **2008**, *27*, 1470−1478.

(12) Pfirrmann, S.; Limberg, C.; Herwig, C.; Knispel, C.; Braun, B.; Bill, E.; Stösser, R. *J. Am. Chem. Soc.* **2010**, *132*, 13684−13691.

(13) (a) Elder, M. *Inorg. Chem.* **1970**, *9*, 762−767. (b) Takao, T.; Yoshida, S.; Suzuki, H.; Tanaka, M. *Organometallics* **1995**, *14*, 3855−3868. (c) Takao, T.; Yoshida, S.; Suzuki, H. *Chem. Lett.* **2001**, *30*, 1100−1101. (d) Ohki, Y.; Kojima, T.; Oshima, M.; Suzuki, H. *Organometallics* **2001**, *20*, 2654−2656. (e) Tanabe, M.; Ito, D.; Osakada, K. *Organometallics* **2007**, *26*, 459−462. (f) Heiden, Z. M.; Zampella, G.; De Gioia, L.; Rauchfuss, T. B. *Angew. Chem.* **2008**, *120*, 9902−9905. (g) Alvarez, M. A.; Alvarez, M. P.; Carreño, R.; Ruiz, M. A.; Bois, C. *J. Organomet. Chem.* **2011**, *696*, 1736−1748.

(14) (a) Beck, R.; Johnson, S. A. *Organometallics* **2012**, *31*, 3599−3609. (b) Zell, T.; Schaub, T.; Radacki, K.; Radius, U. *Dalton Trans.* **2011**, *40*, 1852−1854. (c) Iluc, V. M.; Hillhouse, G. L. *Tetrahedron* **2006**, *62*, 7577−7582. (d) Iluc, V. M.; Hillhouse, G. L. *J. Am. Chem. Soc.* **2010**, *132*, 11890−11892.

(15) (a) Mullica, D. F.; Sappenfield, E. L.; Hampden-Smith, M. J. *Polyhedron* **1991**, *10*, 867−872. (b) Simons, R. S.; Sanow, L. M.; Galat, K. J.; Tessier, C. A.; Youngs, W. J. *Organometallics* **2000**, *19*, 3994−3996. (c) Chan, D.; Duckett, S. B.; Heath, S. L.; Khazal, I. G.; Perutz, R. N.; Sabo-Etienne, S.; Timmins, P. L. *Organometallics* **2004**, *23*, 5744−5756. (d) West, N. M.; White, P. S.; Templeton, J. L.; Nixon, J. F. *Organometallics* **2009**, *28*, 1425−1434.

(16) (a) Chen, W.; Shimada, S.; Tanaka, M.; Kobayashi, Y.; Saigo, K. *J. Am. Chem. Soc.* **2004**, *126*, 8072−8073. (b) Tsay, C.; Peters, J. C. *Chem. Sci.* **2012**, *3*, 1313−1318.

(17) MacMillan, S. N.; Hill Harman, W.; Peters, J. C. *Chem. Sci.* **2014**, *5*, 590−597.

(18) Fryzuk, M. D.; Rosenberg, L.; Rettig, S. J. *Organometallics* **1996**, *15*, 2871−2880.

(19) (a) Tamao, K.; Miyake, N.; Kiso, Y.; Kumada, M. *J. Am. Chem. Soc.* **1975**, *97*, 5603−5605. (b) Bheeter, L. P.; Henrion, M.; Brelot, L.; Darcel, C.; Chetcuti, M. J.; Sortais, J.-B.; Ritleng, V. *Adv. Synth. Catal.* **2012**, *354*, 2619−2624. (c) Porter, T. M.; Hall, G. B.; Groy, T. L.; Trovitch, R. J. *Dalton Trans.* **2013**, *42*, 14689−14692. (d) Zheng, J.; Darcel, C.; Sortais, J.-B. *Catal. Sci. Technol.* **2013**, *3*, 81−84. (e) Miller, Z. D.; Li, W.; Belderrain, T. R.; Montgomery, J. *J. Am. Chem. Soc.* **2013**, *135*, 15282−15285. (f) Chakraborty, S.; Krause, J. A.; Guan, H. *Organometallics* **2009**, *28*, 582−586. (g) Tran, B. L.; Pink, M.; Mindiola, D. J. *Organometallics* **2009**, *28*, 2234−2243. (h) Postigo, L.; Royo, B. *Adv. Synth. Catal.* **2012**, *354*, 2613−2618. (i) Marciniec, B.; Maciejewski, H.; Rosenthal, U. *J. Organomet. Chem.* **1994**, *484*, 147−151. (j) Marciniec, B.; Maciejewski, H.; Kownacki, I. *J. Mol. Catal. A* **1998**, *135*, 223−231. (k) Maciejewski, H.; Marciniec, B.; Kownacki, I. *J. Organomet. Chem.* **2000**, *597*, 175−181. (l) Chaulagain, M. R.; Mahandru, G. M.; Montgomery, J. *Tetrahedron* **2006**, *62*, 7560−7566. (m) Cornella, J.; Gómez-Bengoa, E.; Martin, R. *J. Am. Chem. Soc.* **2013**, *135*, 1997−2009.

(20) (a) Rosenthal, U.; Nauck, C.; Arndt, P.; Pulst, S.; Baumann, W.; Burlakov, V. V.; Görls, H. *J. Organomet. Chem.* **1994**, *484*, 81−87. (b) Sgro, M. J.; Stephan, D. W. *Dalton Trans.* **2010**, *39*, 5786−5794.

(21) (a) Becke, A. D. *J. Chem. Phys.* **1993**, *98*, 5648−5652. (b) Lee, C.; Yang, W.; Parr, R. G. *Phys. Rev. B* **1988**, *37*, 785−789. (c) Ditchfield, R.; Hehre, W. J.; Pople, J. A. *J. Chem. Phys.* **1971**, *54*, 724−728. (d) Hehre, W. J.; Ditchfield, R.; Pople, J. A. *J. Chem. Phys.* **1972**, *56*, 2257−2261. (e) Hariharan, P. C.; Pople, J. A. *Theor. Chim. Acta* **1973**, *28*, 213−222.

DOI: 10.1021/jacs.5b03092
J. Am. Chem. Soc. XXXX, XXX, XXX−XXX